INNOVATIVE MECHANICAL ENGINEERING **ISSN 2812-9229 (Online)**
University of Niš, Faculty of Mechanical Engineering
VOL. 1, NO 3, 2022, PP. 49 - 60

Original scientific paper *

THE HORIZONTAL CONVECTION OF AN INCLINED VISCOUS FLUID FLOW

Miloš Jovanović[1], Saša Milanović[1], Živan Spasić[1]

[1]University of Niš, Faculty of Mechanical Enineering, A. Medvedeva 14, Niš, Serbia

Abstract. *The paper presents the results of a numerical simulation for the viscous fluid flow in a slot with cosinusoidal temperature distribution on the lower plate with the increasing slope of the plates with respect to the horizontal line. The numerical simulation is performed using the Fourier Galerkin method in the x-axis direction and the Chebyshev collocation method in the y-axis direction. The stream function-vorticity formulation of the Navier-Stokes equation in the Oberbeck-Boussinesq approximation is used. The uniform Rayleigh number Ra_{uni}=250 and the periodic Rayleigh number value of Ra_p=15,30 is employed in the numerical simulation for the fluid with Pr=7 (water). The horizontal convection known as thermal drift is observed at the angle of inclination $0<\gamma<5°$ for Ra_p=15 and $0<\gamma<15°$ for Ra_p=30. The stream function values are compared with the similar values for different combinations of $Ra_{uni,}$ Ra_p values. This comparison shows a different behavior of the averaged Nusselt and the friction coefficient number for these situations. The results suggest that the ratio between Ra_{uni} and Ra_p is very important for the heat and momentum transfer between the plates. In the first two cases we have optimal value of heat transfer when $\gamma=10^o$, but for Ra_{uni}=500 and Ra_p=30 the maximal value of $Nu_{,av}$ is obtained for $\gamma=0^o$.*

Key words: *Inclined fluif flow, Natural convection, Subcritical condition, Heat transfer intensification Numerical simulation*

1. INTRODUCTION

When the heating intensity is below the critical threshold required for the onset of Rayleigh-Bénard convection (RBC), heat transport across a horizontal fluid layer uniformly heated from below is driven by conduction, placing a limit on its magnitude. The critical conditions required to achieve this critical threshold are well known [1,2]. A methodology to increase the heat flow using the spatial heating non-uniformities is proposed. The non-uniformities create convection whose pattern is dictated by the heating pattern. This convection supplements the conductive heat transport. It has been shown that the effectiveness of this convection, the primary convection, is a strong function of the

*Received: December 09, 2022 / Accepted December 27, 2022.
Corresponding author: Miloš Jovanović
University of Niš, Faculty of Mechanical Engineering
E-mail: milos.jovanovic@masfak.ni.ac.rs

heating wave number and it may increase the heat flux by up to ten times compared to the conductive state if the most effective heat wave number is used [3].

Convection occurs from the conductive state when critical conditions are exceeded [4] and it changes the heat flow character in qualitative terms. These critical conditions are expressed in terms of the critical Rayleigh number Ra_{cr}, with secondary flow occurring when $Ra>Ra_{cr}$. RBC has the form of rolls and is characterized by a linear neutral stability curve with a well-defined minimum. It identifies the critical Rayleigh number and the critical wave vector, with the onset conditions independent of the Prandtl number.

The explicit estimate for maximum heat transfer has been recently published [5]. The use of more intense heating leads to secondary bifurcations and the onset of either skewed-varicose instability, the Eckhaus instability, or the zig-zag instability [6,7], described by using the so-called Busse balloon. Linear stability theory does not offer any guidelines regarding the spontaneous pattern selection which, in most experiments, is determined by secondary effects. A large enough heating intensity leads to turbulent RBC [8-10]. The effects of geometric non-uniformities on such convections have been the subject of recent studies [11].

Inhomogeneities of the plate geometry can affect the onset conditions [12-14]. The detailed analysis and identifications of the relevant mechanisms are not available. Two-dimensional convection rolls have been observed for subcritical conditions $Ra<Ra_{cr}$ for the lower plate being augmented with thin stripes. The amplitude of these rolls grew with Ra until they were destabilized by a mechanism which depended on the ratio between the wave number of the imposed modulation and the critical wave number of the RBC, producing a variety of three-dimensional patterns [12,13]. Recent studies have shown that the state of conduction does not exist only in the presence of geometric modulations, and a natural convection sets in regardless of the heating intensity [15]. The properties of this convection are expected to have a strong effect on the secondary states. Temperature non-uniformities also affect the onset conditions [16], as well as create their own convection, which occurs regardless of the heating intensity [17-19].

2. MATHEMATICAL MODEL

The differential equations that govern the viscous fluid flow in a slot with an inclination to the horizontal line are

$$\frac{\partial \vec{\omega}}{\partial t} + \vec{v} \cdot \nabla \vec{\omega} = \nabla \times \vec{F} + \nu \Delta \vec{\omega} \tag{1}$$

$$\vec{\omega} + \Delta \vec{\psi} = 0 \tag{2}$$

$$\frac{\partial T}{\partial t} + \vec{v} \cdot \nabla T = \frac{\lambda}{\rho c_p} \Delta T + \dot{q} \tag{3}$$

with the appropriate boundary conditions

$$
\begin{aligned}
&y=\frac{H}{2},\ \ \psi=\int_{-1}^{1}u\left(x,y\right)dy,\ \ \frac{\partial\psi}{\partial y}=0,\ T=T_{w1},\\
&y=-\frac{H}{2},\ \ \psi=0,\ \ \frac{\partial\psi}{\partial y}=0,\ \ \ T=T_{w2}+\frac{T_p}{2}\cos\alpha x.
\end{aligned}
\tag{4}
$$

The initial conditions for the variables $\omega(x,y,t)$, $\psi(x,y,t)$, $T(x,y,t)$, $\gamma(t)$ read

$$
\begin{aligned}
t=0,\ \ &\psi\left(x,y\right)=0,\ \ \ \ \omega\left(x,y\right)=0,\\
&T\left(x,y\right)=T_{w1}+\left(\frac{H}{2}-y\right)\frac{\Delta T}{H},\\
&0\le x\le L,\ \ \ \ -\frac{H}{2}\le y\le\frac{H}{2}.
\end{aligned}
\tag{5}
$$

where $\Delta T = T_{w2} - T_{w1}$ is the temperature difference between the homogeneous part of the lower wall temperature T_{w2} and the homogeneous temperature of the upper wall T_{w1}. In Eqs. (1-5) the following notation is used: $\vec{v}$ - velocity vector, $\vec{\omega}$- vorticity vector, $\vec{F}$ - volumetric force per unit mass, $\vec{\psi}$ -stream function vector, T- temperature, ν-kinematic viscosity (momentum diffusivity), $\kappa=\lambda/\rho c_p$ -thermal diffusivity, λ-thermal conductivity, ρ-fluid density, c_p-specific heat at constant pressure, $\dot{q}$ -heat flux per unit volume, $\Delta=\nabla\cdot\nabla$ -Laplacian of a scalar or vector field, as a scalar product of the nabla operator ∇ with itself. In Fig. (1) we have designated: H-the distance between the parallel plates, L-the length of the periodic slot filled with the viscous fluid, T_{w1}- the temperature of the upper colder plate, T_{w2}- the homogeneous part of the warmer lower plate temperature, T_p -the peak to peak amplitude of the lower plate periodic temperature, α - the periodic temperature wave number.

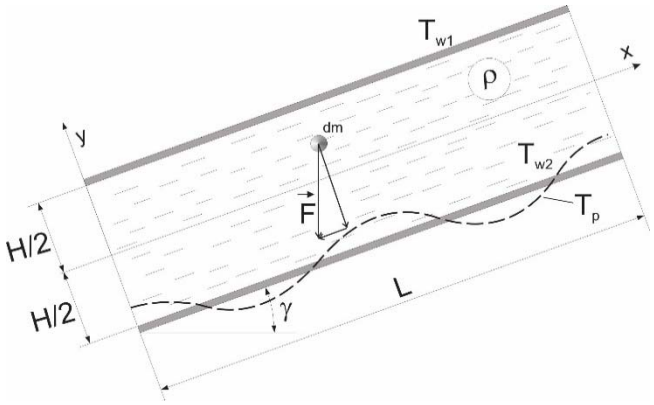

Fig. 1 Physical model of the viscous fluid flow with an inclination angle γ.

In the Oberbeck-Boussinesq approximation, density changes only in the force term of the momentum equation according to $V = V_0\ [1+\beta(T-T_0)]$. β=1/T - thermal expansion coefficient (~$3\cdot10^{-3}$ for gases and ~$5\cdot10^{-4}$[K^{-1}] for liquids), so for m=const. we have

$$\frac{\rho}{\rho_0}=\frac{m/V}{m/V_0}=\frac{1}{1+\beta\left(T-T_0\right)}\approx 1-\beta\left(T-T_0\right). \tag{6}$$

After substituting Eq. (6) into the buoyancy force term in the vorticity transport Eq. (1), which only considers the fluid density variations, we obtain

$$\vec{F}\approx\left[1-\beta\left(T-T_0\right)\right]g\left(-\sin\gamma\,\vec{i}-\cos\gamma\,\vec{j}\right). \tag{7}$$

Here we have anticipated $T_0 = T_{w1}$ and that the plates can be parallel to each other but with some inclination angle γ to the horizontal line. The results of numerical simulation in this paper are limited to the case where γ=0º,5º,10º,15º,20º, and *x,y* are the longitudinal and transverse coordinate, and *g*-gravity acceleration. In order to obtain the nondimensional form of the previous equations, we have used the following expressions

$$\begin{aligned}&\psi=\kappa\psi^*,\ \ \omega=\frac{\kappa}{H^2}\omega^*,\ T^*=\frac{T-T_{w1}}{T_{w2}-T_{w1}},\ t=\frac{H^2}{\kappa}t^*,\\ &x=\frac{L}{2\pi}x^*\left(0\le x^*\le 2\pi\right),\ \ y=\frac{H}{2}y^*\left(-1\le y^*\le 1\right).\end{aligned} \tag{8}$$

We have chosen the length scales in the direction of the *x*- and *y*-axes in accordance with the domain of basic functions, using the Fourier expansion in the *x*-direction and the Chebyshev expansion in the *y*-direction. We have also used the following nondimensional parameters

$$\begin{aligned}&Ra_{uni}=\frac{g\beta\left(T_{w2}-T_{w1}\right)H^3}{\kappa\,\nu},\ Ra_p=\frac{g\beta T_p H^3}{\kappa\,\nu},\ \ a=\frac{\pi H}{L},\ \ \kappa=\frac{k}{\rho c_p},\ \ Pr=\frac{\nu}{\kappa}.\\ &c_f\left(x^*\right)=\frac{2}{\mathrm{Re}}\left(\frac{\partial u^*}{\partial y^*}\right)_{y^*=-1},\quad c_{f,av}=\frac{1}{\lambda}\int_0^{\lambda}c_f\left(x^*\right)dx^*,\ \ \lambda=\frac{2\pi}{\alpha}\\ &Nu\left(x^*\right)=\left(\frac{\partial T^*}{\partial y^*}\right)_{y^*=-1},\qquad Nu_{av}=\frac{1}{\lambda}\int_0^{\lambda}Nu\left(x^*\right)\,dx^*.\end{aligned} \tag{9}$$

In the expressions above Ra_{uni} and Ra_p represent the uniform and periodic Rayleigh numbers measuring the intensity of the uniform and periodic heating component, *Pr* is the Prandtl number as a ratio of the momentum diffusivity ν to thermal diffusivity κ, *a* is the aspect ratio of vertical to horizontal slot dimensions, *Re* is the Reynolds number, λ is the heating wavelength and α is the periodic heating wavenumber on the lower wall. The field equations, which consist of vorticity transport Eq. (1), the definition of vorticity substituting the continuity Eq. (2), and thermal energy transport Eq. (3), now have the following nondimensional form

$$\frac{\partial \boldsymbol{\omega}^*}{\partial t^*}+4a\left(\frac{\partial \boldsymbol{\psi}^*}{\partial y^*}\frac{\partial \boldsymbol{\omega}^*}{\partial x^*}-\frac{\partial \boldsymbol{\psi}^*}{\partial x^*}\frac{\partial \boldsymbol{\omega}^*}{\partial y^*}\right)=2RaPr\left(a\frac{\partial T^*}{\partial x^*}\cos\boldsymbol{\gamma}-\frac{\partial T^*}{\partial y^*}\sin\boldsymbol{\gamma}\right)+$$
$$+4Pr\left(a^2\frac{\partial^2\boldsymbol{\omega}^*}{\partial x^{*2}}+\frac{\partial^2\boldsymbol{\omega}^*}{\partial y^{*2}}\right), \tag{10}$$

$$\boldsymbol{\omega}^*+4\left(a^2\frac{\partial^2\boldsymbol{\psi}^*}{\partial x^{*2}}+\frac{\partial^2\boldsymbol{\psi}^*}{\partial y^{*2}}\right)=0, \tag{11}$$

$$\frac{\partial T^*}{\partial t^*}+4a\left(\frac{\partial \boldsymbol{\psi}^*}{\partial y^*}\frac{\partial T^*}{\partial x^*}-\frac{\partial \boldsymbol{\psi}^*}{\partial x^*}\frac{\partial T^*}{\partial y^*}\right)=4\left(a^2\frac{\partial^2 T^*}{\partial x^{*2}}+\frac{\partial^2 T^*}{\partial y^{*2}}\right)+q^*. \tag{12}$$

The boundary and initial conditions in the non-dimensional form are the following

$$y^*=1,\quad \boldsymbol{\psi}^*=\int_{-1}^{1}u^*\left(y^*\right)dy^*,\quad \frac{\partial\boldsymbol{\psi}^*}{\partial y^*}=0,\quad T^*=0,\quad 0<t^*\le\boldsymbol{\pi}, \tag{13a}$$

$$\begin{aligned}
&y^*=-1,\quad \boldsymbol{\psi}^*=0,\quad \frac{\partial\boldsymbol{\psi}^*}{\partial y^*}=0,\quad T^*=1+\tfrac{1}{2}T_p^*\left(t^*\right)\cos\left(\boldsymbol{\alpha}x^*+\Omega\right),0<t^*\le\boldsymbol{\pi}/2,\\
&t^*=0,\quad \boldsymbol{\psi}^*\left(x^*,y^*\right)=0,\quad \boldsymbol{\omega}^*\left(x^*,y^*\right)=0,\quad T^*\left(x^*,y^*\right)=\tfrac{1}{2}\left(1-y^*\right),\\
&0\le x^*\le 2\boldsymbol{\pi},\quad -1\le y^*\le 1.
\end{aligned} \tag{13b}$$

If the plates are inclined with respect to the horizontal plane by the angle γ, the value of net flow rate in the *x*-axis direction $\boldsymbol{\psi}^*\left(y^*=1\right)=\int_{-1}^{1}u^*\left(x^*,y^*\right)dy^*=g_+\left(t^*\right)$ must be computed, and it usually has a negative value for γ>0, since the velocity component $u^*(x^*,y^*)$ is predominatly negative for *x*=const. and for positive angle γ. The function $g_+\left(t^*\right)$ is the nondimensional volumetric flow rate through the channel's cross-section. Here we designate $T_p^*=T_p/\left(T_{w2}-T_{w1}\right)$ as the nondimensional periodic temperature. The initial conditions for the fields of stream function, vorticity and velocity are equal to zero, but we anticipate linear temperature distribution between the plates, since at that instant of time the temperature distribution is homogeneous at both plates for the constant value of Ra_{uni}. The boundary conditions at the lower plate are applied gradually over a certain period of time $0<t^*<\pi/2$, until the values of Ra_{uni} and Ra_p are achieved.

$$\begin{aligned}
&T^*\left(y^*\right)=\tfrac{1}{2}\left(1-y^*\right),\qquad -1\le y^*\le 1,\qquad t^*=0,\\
&Ra_p(t^*)=Ra_p\sin\left(t^*\right),\ Ra_{uni}(t^*)=Ra_{uni}\sin\left(t^*\right),\ \boldsymbol{\gamma}=0,\quad 0\le t^*\le\boldsymbol{\pi}/2,\\
&\boldsymbol{\gamma}^{n+1}=\boldsymbol{\gamma}^n+\Delta\boldsymbol{\gamma},\quad 0\le\boldsymbol{\gamma}\le 20\boldsymbol{\pi}/180,\ Ra_p=const.\ \boldsymbol{\pi}/2\le t^*\le\boldsymbol{\pi}.
\end{aligned} \tag{14}$$

In order to achieve such a numerical simulation, we use the four time-level, third order temporal discretizing procedure AB/BDI3 [20]. This semi-implicit method applies

generally to nonlinear Eqs. (10) and (12) where the coefficients of the linear operator are constant. This is the case of Navier-Stokes equations for incompressible fluids with constant viscosity, and also its counterpart vorticity transport Eq. (10). This linear term is considered implicitly, and the nonlinear term is explicit, so that the resulting discrete operator is time-independent and can be inverted or diagonalized in a pre-processing stage, before the start of time-integration. Such time discretization is commonly associated with Fourier and Chebyshev spatial approximations. The details of the spatial and time discretization procedure have been described in [20-22]. Further on, we drop * for the nondimensional notation, but all variables are considered as dimensionless.

3. THE RESULTS OF NUMERICAL SIMULATION

Eqs. (10-12) with boundary and initial conditions, Eq. (13), have been solved numerically by using the influence matrix method [23] for determination of boundary conditions for vorticity, since they are unknown in the above Eq. (13). The in-house numerical code has been developed in MATLAB. The results of numerical simulation are displayed in this section. The Fourier-Galerkin spectral method has given an accurate spatial resolution with $K=N_x/2=64$ modes, and $N_y=128$ as Gauss-Lobatto-Chebyshev points, and for temporal discretization we have used the time step $\Delta t=\pi/300$, and the angle of inclination increment $\Delta\gamma=20\pi/180\cdot 1/150=\pi/1350$. The temperature field must be calculated at the time level $n+1$, i.e. where $\hat{\Theta}_k^{n+1}$ are the temperature Fourier modes, so the implicit methods must be used. The used time step $\Delta t=\pi/300$ is sufficiently small so that the numerical diffusion error can be neglected. All elements of discretization have spectral accuracy, so the global accuracy of the computations is controlled by changing the number of Fourier modes and Chebyshev polynomials appropriately. All the results presented in this paper were obtained with an accuracy of at least four digits.

We can see the dimensionless stream function and streamlines (ψ=const.) for subcritical Rayleigh numbers $Ra_{uni}=250$, and two different values for periodic Rayleigh numbers $Ra_p=15$ and $Ra_p=30$, aspect ratio $a=1$, where the critical value for this flow for both plates with homogeneous temperature distribution is $Ra_{cr}=1708$ for the wave number of disturbance $\alpha_{cr}=3.16$. So, for this value of Ra_{uni}, there should not be any flow, for uniform temperature distribution at the lower wall ($Ra_p=0$).

Since we have the cosinusoidal component of temperature distribution at the lower plate – the so-called periodic temperature T_p, with dimensionless value $Ra_p\neq 0$, the fluid motion sets in regardless of the value of Ra_{uni}, if it does or does not reach the critical value Ra_{cr}. Fig. (2) shows these five scalar fields for five different angles of inclination $\gamma=0$, $5\pi/180$, $10\pi/180$, $15\pi/180$, $20\pi/180$ at the instant of time $t=\pi/2$, $5\pi/8$, $6\pi/8$, $7\pi/8$, π, respectively.

The wave number of periodic temperature distribution at the lower plate is $\alpha=2$ for this simulation, and there is no temperature phase shift ($\Omega=0$) on the lower wall. The numerical results for stream function are similar in the spatial distribution, but not in their intensities for different inclination angles γ.

Hot spots, locations where periodic temperature on lower plate attains its maximum, are located at $x^*=0,\pi,2\pi=n\cdot 2\pi/\alpha$, for n=0,1,2 and *cold spots* positions where the periodic component of temperature attains its minimum are located in $x^*=\pi/2,3\pi/2=(2n+1)\cdot\pi/\alpha$ for n=0,1 in accordance with the temperature distribution given by (12) and periodic

temperature wave number α=2 on the lower wall. In the instant of time t=π/2, when γ=0, Ra_{p} and Ra_{uni} attain their maximal values according to Eq. (14) and remain constant for t>π/2. In Fig. (2.a and b), where the dimensionless stream function distribution $\psi(x,y,t)$ is displayed, we can see two pairs of rolls which rotate in the clockwise (blue area) and counterclockwise directions (orange area). Just above these *hot spots*, the fluid motion is directed upwards, hits the upper cooler surface, splits into two streams parallel with plates, gets cooled and its density gets higher and then drops from the upper to the lower plate at x*=π/2,3π/2 in *cold spots*, where the temperature achieves its minimum according to Eq. (12). The fluid rises above the *hot spots* and descends toward the *cold spots* forming counter-rotating rolls displayed in Fig. (2.a) for Ra=250 and Ra_p=15 and in Fig. (2.b) for Ra=250 and Ra_p=30. The nondimensional stream function intensity $\psi(x,y,t)$ can be compared for five different inclination angles γ=0°,5°,10°,15°,20°, at the corresponding instant of time t=π/2, 5π/8, 6π/8, 7π/8, π, respectively, see Fig. 2 (a,c,e,g,i), after the periodic Rayleigh number achieves its value Ra_p =15 and Ra_{uni}=250 at the instant of time t=π/2. Two pairs of rolls rotate with the same intensity for γ=0, but in the opposite direction, displayed in Fig. 2a for Ra_p =15 and in Fig. 2b for Ra_p =30, clockwise - negative direction (blue color) and counterclockwise - positive direction (orange color), and the extreme values of stream function are ψ_{max}(2.307,0.0)=0.1306, ψ_{min}(3.902,0.0)=−0.1306 for Fig. 2a and ψ_{max}(2.319,0.0)=0.2565, ψ_{min}(3.89,0.0)=−0.2565 for Fig. 2 b.

The borders between rolls overlap with the peaks and bottoms of fluid temperature distribution. They are depicted in Fig. 5a and Fig. 5 b, which also overlap with the hot and cold spots on the lower wall. In Fig. 2b, d, f, h, j we can see stream function distribution and streamlines (ψ=const.) for Ra_p =30 and Ra_{uni}=250 for five different inclination angles γ=0°,5°,10°,15°,20°, at the corresponding instant of time t=π/2, 5π/8, 6π/8, 7π/8, π, respectively. We see in Fig. 2d, f that counterclockwise rotating rolls (orange one) get weaker, lose its intensity of rotation and shrink in the x-direction, but the clockwise (blue one) rotating rolls get stronger, increase their magnitude and extend in the x-direction with the increasing angle of inclination γ. The convection intensity represented by these values of stream function is almost double in value ψ_{max}(2.319,0.0)=0.2565 for Ra_p=30, than for Ra_p=15 when it is ψ_{max}(2.307,0.0)=0.1306 for γ=0° which can be noticed on the right hand side color bar. When the slope of the plates is increased with respect to the horizontal line to the value γ=5°, Fig. 2d, the upward fluid flow above the hot spots splits into two branches when it hits the upper plate. The first one goes left and downward and the second one goes right and upward beneath the upper plate. When the inclination angle γ is positive, i.e. in the counterclockwise direction, more fluid goes right than left, because the warmer fluid with less density goes up beneath the plate, since the buoyancy force in this direction is stronger. This is the reason why with the increasing inclination angle γ, positive rotating rolls shrink, and negative rotating rolls expand. The second consequence is that the center of the positive rolls moves downward and both rolls move to the left in the negative x-axis direction, due to the component of buoyancy force parallel to the plates for γ>0. Fig. 3d displays patterns with the flow topology consisting of sets of rolls separated from each other by a stream tube weaving up and down and carrying fluid in the negative x-direction, for our case γ>0. In Fig. 3f the positive rotating rolls can be barely noticed with

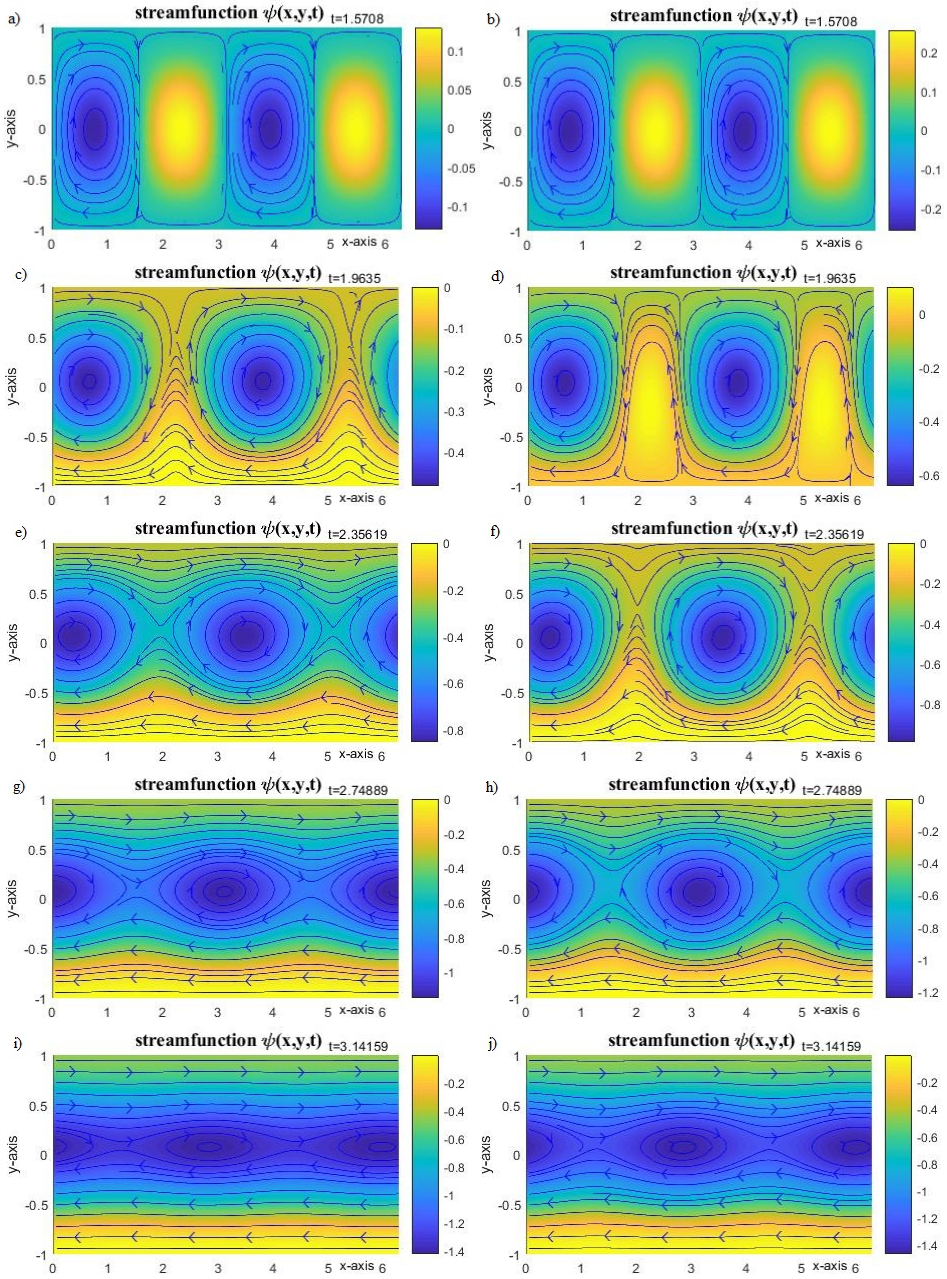

Fig. 2 Stream function and streamlines distribution for Ra_{uni}=250, Ra_p=15, different angles γ, a) γ=0°, c) γ=5°, e) γ=10°, g) γ=15°, i) γ=20°, and distribution for Ra_{uni}=250, Ra_p=30, for different angles γ, b) γ=0°, d) γ=5°, f) γ=10°, h) γ=15°, j) γ=20°

their centers near the lower wall at positions $x\approx2$ and $x\approx5.14$, and negative rotating central rolls expand almost to whole central area of the slot. In Fig. 3f the fluid almost stops weaving up and down and is restricted to the slot part close to the lower wall to stream in the negative x-direction and close to the upper wall where the stream flows in the positive x-axis direction, which is more evident in Fig. 3h, j.

The intensities of convection displayed by ψ_{min} indicate that with the increasing slope angle γ, this extreme value of stream function gets higher absolute values, and the convection in the slot middle is intensified before it gets the quasi-one-dimensional flow pattern at the higher values of γ, Fig. 2i, j. The horizontal convection – known as thermal drift [24], can be seen only in Fig. 2d as weaving up and down between the rolls in the negative x-direction and cannot be seen in Fig. 2c since the positive rotating rolls almost disappeared at $\gamma=5°$ and the center of these two baby rolls is very close to the lower wall and can barely be seen in Fig. 2c. The horizontal convection could probably be better presented for the value of $Ra_p=15$ for smaller values of γ, better to say for the value $0<\gamma<5°$, since at this value of Ra_p the process of shrinking the positive rotating rolls and moving of their centers to the lower wall is almost completed for $0<\gamma<5°$.

For a higher value $Ra_p=30$ and the same $Ra_{uni}=250$, this process is completed for the interval $0<\gamma<10°$, but for $Ra_p=30$ and the same $Ra_{uni}=500$ [25], the process of shrinking the positive rotating rolls and expanding the negative rotating rolls is extended to the interval $0<\gamma<20°$ when at $\gamma=20°$ the counter-clockwise rotating rolls become baby rolls near the lower wall and finally disappear with a further increment of the inclination angle γ.

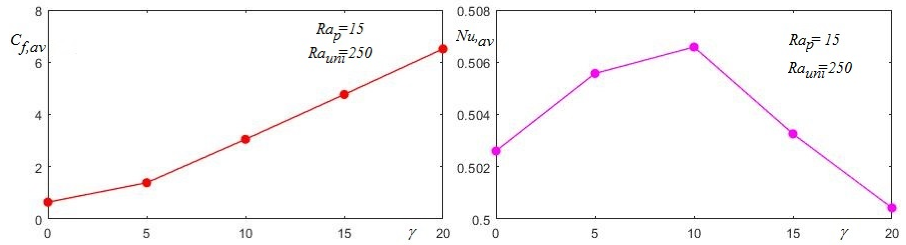

Fig. 3 Distribution of Nusselt average number Nu_{av} and average friction coefficient $C_{f,av} \times Re/2$ for five different angles of inclination $\gamma=0°,5°,10°,15°,20°$ for $Ra_{uni}=250$, $Ra_p=15$.

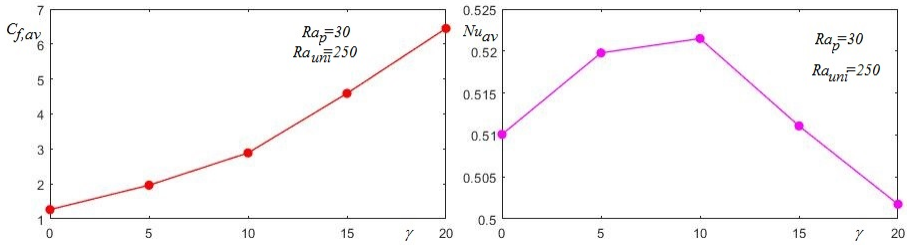

Fig. 4 Distribution of Nusselt average number Nu_{av} and average friction coefficient $C_{f,av} \times Re/2$ for five different angles of inclination $\gamma=0°,5°,10°,15°,20°$f or $Ra_{uni}=250$, $Ra_p=30$.

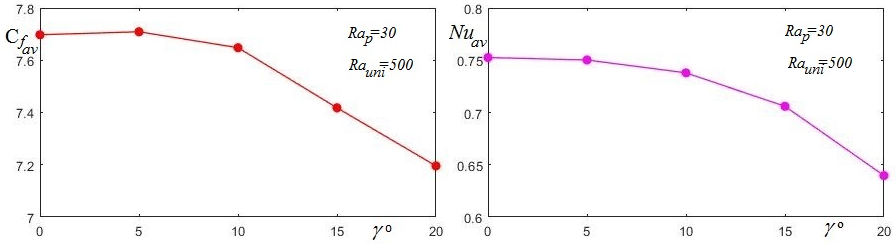

Fig. 5 Distribution of Nusselt average number Nu_{av} and average friction coefficient $C_{f,av} \times Re/2$ for five different angles of inclination γ=0°,5°,10°,15°,20°for Ra_{uni}=500, Ra_p=30.

Fig. 3 shows the Nusselt and friction coefficient average number in dependence of the inclination angle γ for Ra_p=15 and Ra_{uni}=250. We can see that $C_{f,av}$ is a monotonic increasing function of γ, and the $Nu_{,av}$ is an increasing function for the interval 0≤γ≤10°, but a decreasing function for 10<γ≤20°. The Nusselt number achieves the optimal value for γ=10°. Fig. 4 shows the functions $C_{f,av}(\gamma)$ and $Nu_{,av}(\gamma)$ for Ra_p=30 and Ra_{uni}=250. The distribution of functions $C_{f,av}(\gamma)$and $Nu_{,av}$ (γ) is very similar with the previous one. The slope of the function $C_{f,av}(\gamma)$ gets higher values for interval 10≤γ≤20°, than for 0≤γ≤10°. This value γ=10° is the optimal inclination angle for the Nusselt number, where it achieves its maximal value. The situation is quite different if we double the value of the uniform Rayleigh number Ra_{uni}, as it is shown in Fig. 5.

In this figure we can notice that $C_{f,av}(\gamma)$ achieves its maximum for γ=5°, and afterwards it is a monotonic decreasing function with respect to γ. In the same figure we see that $Nu_{,av}(\gamma)$ is a monotonic decreasing function on the whole domain. We can notice that both tend to decline with the increasing inclination angle γ. Both values have been calculated for the lower plate, where the Nusselt number is displayed in the absolute value, since its values on the lower plate have a negative sign. This can be explained by the fact that thermal energy goes from the lower to the upper plate, and the lower one loses and the upper one gains thermal energy. We can see some small increment of the friction coefficient for the angle of inclination γ=5°. The results are in accordance with the results displayed in [26, 27]. The function $Nu_{,av}(\gamma)$ gets slightly higher values for Ra_p=30 than for Ra_p=15 if Ra_{uni}=250 in both cases, but if we double the value of the uniform Rayleigh number to Ra_{uni}=500, the increase in the values of function $Nu_{,av}(\gamma)$ is significant and amounts to almost 50%. The ratio between Ra_{uni}/Ra_p is an obviously significant control parameter in obtaining the optimal value of $Nu_{,av}$,$C_{f,av}$ and $ReC_{f,av}(\gamma)/2$.

4. CONCLUSIONS

We have discussed the system's response when the uniform and periodic heating components are combined. The very small periodical heating Ra_p=15,30 together with uniform heating Ra_{uni}=250, which is below the critical value Ra_{cr}=1708 for homogeneous temperature distribution on the plates, forms the flow patterns presented in Fig. 2 for fields of stream function. The aspect ratio $a=\pi H/L$ has been chosen to be a=1, and its influence on convection intensity should be investigated in detail in further research.

Heating non-uniformities represent a wider class of problems which has been studied on a case by case basis. The temperature non-uniformities on the lower plate create horizontal and vertical temperature gradients which result in horizontal density variations that create motions frequently referred to as *horizontal convection*. The heating creates horizontal temperature gradients which lead to the formation of vertical and horizontal temperature gradients that in turn lead to the formation of the vertical and horizontal pressure gradient that drives the fluid motion regardless of the intensity of heating. When the hot spots overlap either with the fluid flow pattern tips or with its bottoms, convection assumes the form of pairs of counter-rotating rolls whose size is dictated by the heating wavelengths. The formation of a net horizontal flow, referred to as *thermal drift*, is observed for all other relative positions of the hot spots and the fluid temperature peaks. Both periodic heating and periodic fluid flow pattern are required for formation of this drift, which can be directed in the positive as well as in the negative horizontal directions depending on the phase difference Ω_{fp} between the heating and the fluid flow patterns.

In our case depending on the negative or positive values of the inclination angle γ, whether the component of gravitational acceleration in the direction of the x-axis is positive or negative (thermal drift is a very strong function of the phase difference), the largest thermal drift occurs for inclination angle $\gamma=10°$ at the instant of time $t=5\pi/8$ for $Ra_p=30$. The combined effect of buoyancy-induced shear flow leads to the creation of convection rolls and gravity-induced shear flow leads to the creation of thermal drift with magnitude depending on the angle of inclination of plates γ and the gravity component in the direction of the x-axis. The flow topology is locked in with the heating pattern but only for small convection intensities ψ_{max}, for low Rayleigh numbers and the angle of inclination $\gamma=0°$. If $\gamma\neq0$ the fluid flow pattern starts sliding in the direction of the gravity component parallel to the x-axis, for the case of $\gamma>0$ it is in the negative and for $\gamma<0$ it is in the positive direction of the x-axis. Fig. 2d displays the fluid flow pattern for the phase shift $\Omega_{fp}\approx\pi/10$, with the flow topology consisting of sets of rolls separated from each other by a stream tube weaving up and down and carrying fluid in the negative x-direction, for our case $\gamma>0°$. We have seen that the most intense convection and the largest thermal drift occur for $\gamma=10°$ at the instant of time $t=5\pi/8$ for $Ra_p=30$. Their intensity increases proportionally to the uniform heating intensity Ra_{uni} and the periodic heating intensity Ra_p. It has been shown that periodic heating and an inclination angle γ are required for the thermal drift formation, which is important for the horizontal flow control in micro-devices. The presence of heating non-uniformities is expected to affect the transition conditions for secondary convection as it has been recently investigated [28, 29].

Acknowledgement: *The paper is a part of the research done within the project of Faculty of Mechanical Engineering in Niš, financially supported by the Ministry of Education, Science and Technological Development of the Republic of Serbia (Contract No.451-03-9/2021-14/200109).*

REFERENCES

1. Rayleigh J.W.S., 1916, *On convection currents in a horizontal layer of fluid, when the higher temperature is on the underside*. Phil. Mag. vol.32, pp. 529-546.
2. Bénard H., 1900, *Les tourbillons cellulaires dans une nappe liquide*. Revue Générale Science Pure et Applique, vol.11, pp.1261-1271.

3. Hossain M.Z., Floryan J.M., 2013, *Heat transfer due to Natural Convection in a Periodically heated Slot*, Journal of Heat Transfer, vol.135, 022503-1.
4. Chilla F., Schumacher J., 2012, *New perspective in turbulent Rayleigh-Bénard convection,* Eur. Phys. J., E 35, pp.58-82.
5. Hassanzadeh P., Chini G.,Doering C., 2014, *Wall to wall optimal transport*, J. Fluid Mech., vol.751, pp. 621-662.
6. Clever R.M., Busse F.H.,1974, *Transition to time-dependant convection*, J. Fluid Mech., vol.65, pp.625-645.
7. Busse F.H.,Clever R.M.,1979, *Instabilities in convection rolls in a fluid of moderate Prandtl number*. J.Fluid Mech.,vol.91,pp.319-335.
8. Ahlers G., Grossman S., Lohse D., 2009, *Heat transfer and large scale dynamics in turbulent Rayleigh-Bénard convection*, *Rev. Mod. Phys.*, vol.81, pp.503-537,
9. Lohse D.,Xia K.Q., 2010, *Small scale properties of turbulent Rayleigh-Bénard convection*, Annu. Rev. Fluid Mech., vol.42, pp.335-364,
10. Toppaladoddi S., Succi S., Wettlaufer J.S., 2015, *Tailoring boundary geometry to optimize heat transport in turbulent convection.* Eur. Phys. Lett. A, vol. 111, 44005,
11. Golushkin D., Doering C.R., 2016, *Bounds for convection between rough boundaries*, J. Fluid Mech., vol.804, pp.370-386,
12. McCoy J.H., Brunner W., Pesch W., Bodenschatz E., 2008, *Self-organization of topological defects due to applied constraints*, Phys. Rev. Lett., vol.101, 254102.
13. Seiden G., Weiss S., Pesch W., Mc Coy J.H., Bodenschatz E., 2008 ‚*Pattern forming system in presence of different symmetry-breaking mechanism*, Phys. Rev. Lett., vol.101, 214503.
14. Weiss S., Seiden G., Bodenschatz E., 2012, *Pattern formation in spatially forced thermal convection*, New J. Physics, vol.14, 053010.
15. Abtahi A., Floryan J.M., 2017, *Natural convection in a corrugated slots*, J.Fluid Mech., Vol.815, pp.537-569.
16. Freund G., Pesch W., Zimmerman W., 2011, *Rayleigh-Bénard convection in the presence of spatial temperature modulation*, J. Fluid Mech., vol.673, pp.318-348.
17. Hossain M.Z., Floryan J.M., 2013, *Instability of natural convection in a periodically heated layer*. J. Fluid Mech., vol.733, pp.33-67.
18. Cheong H., Siri Z., Sivasanakran S. 2013, *Effect of aspect ratio on natural convection in an inclined rectangular enclosure with sinusoidal boundary condition*, International Communications in Heat and Mass Transfer, vol.45, pp.75-85.
19. Hossain M.Z., Floryan D., Floryan J.M., 2012, *Drag reduction due to spatial thermal modulation*, J.Fluid Mech., vol.713, pp.398-419.
20. Hossain M.Z., Floryan J.M., 2015a, *Mixed convection in periodically heated channel*, J.Fluid Mech., vol.768, pp.51-90.
21. Jovanović M.M., Nikodijević D.J., Nikodijević D.M., 2015, *Rayleigh-Benard convection instability in the presence of spatial temperature modulation on both plates*, International Journal of Non-Linear Mechanics, vol.73, pp.69-74.
22. Vanishree R.K.,Anjana K., 2017, *The Linear and Non-linear Study of Effects of Temperature Modulaton on Double Diffusive Convection in Oldroyd-B Liquids*". Int.J.Appl.Comput.Math,vol.3, suppl.1,p.1095-1117,
23. Chen X., Shih T., Wang B., Chang R., Chen X.,2018, *Nusselt number influenced by expansion/compression, birth/death, and recirculating direction of vortices in elongated enclosures* Inter.Commun.Heat and Mass Transfer, , vol.97, p.110-117.
24. Zhao C., Wang B., Wu J., Chong K., & Zhou Q., 2022, *Suppression of flow reversals via manipulating corner rolls in plane Rayleigh–Bénard convection*. J. Fluid Mech., vol.946, A44.
25. Zhao C., Zhang Y., Wang B., Wu J., Chong K., Zhou Q. 2022, *Modulation of turbulent Rayleigh-Benard convection under spatially harmonic heating*. Physical Review E, 105, 055107.
26. Floryan J.M., Wang W., Panday S., Andrew P. Bassom, 2022, *Natural convection and pattern interaction in a two-dimensional vertical slot*, J. Fluid Mech., vol.946, A20.
27. Hossain M.Z., Floryan J.M., 2022, *Wavenumber lock in and spatial parametric resonance in convection*, J. Fluid Mech., vol.944, A47.
28. Peyret R., Krause E., 2000, *Advanced Turbulent Flow Computations*, CISM courses and lectures No.395, Springer Verlag Wien,
29. Canuto C., Hussaini M.Y., Quarteroni A., Zang T.A., 2007, *Spectral Methods*, *Fundamentals in Single Domain*, Springer Verlag, New York,